

## METHOD

# *n*PoRe: *n*-Polymer Realigner for improved pileup-based variant calling

Tim Dunn<sup>\*</sup>, David Blaauw, Reetuparna Das and Satish Narayanasamy

<sup>\*</sup>Correspondence:

[timdunn@umich.edu](mailto:timdunn@umich.edu)

University of Michigan, Ann Arbor,  
USA

Full list of author information is  
available at the end of the article

## Abstract

Despite recent improvements in nanopore basecalling accuracy, germline variant calling of small insertions and deletions (INDELs) remains poor. Although precision and recall for single nucleotide polymorphisms (SNPs) now exceeds 99.5%, INDEL recall remains below 80% for standard R9.4.1 flow cells. We show that read phasing and realignment can recover a significant portion of false negative INDELs. In particular, we extend Needleman-Wunsch affine gap alignment by introducing new gap penalties for more accurately aligning repeated *n*-polymer sequences such as homopolymers ( $n = 1$ ) and tandem repeats ( $2 \leq n \leq 6$ ). At the same precision, haplotype phasing improves INDEL recall from 63.76% to 70.66% and *n*PoRe realignment improves it further to 73.04%.

**Keywords:** germline variant calling; alignment; *n*-polymer; homopolymer; short tandem repeat; copy number; nanopore sequencing; variable gap penalty

## Background

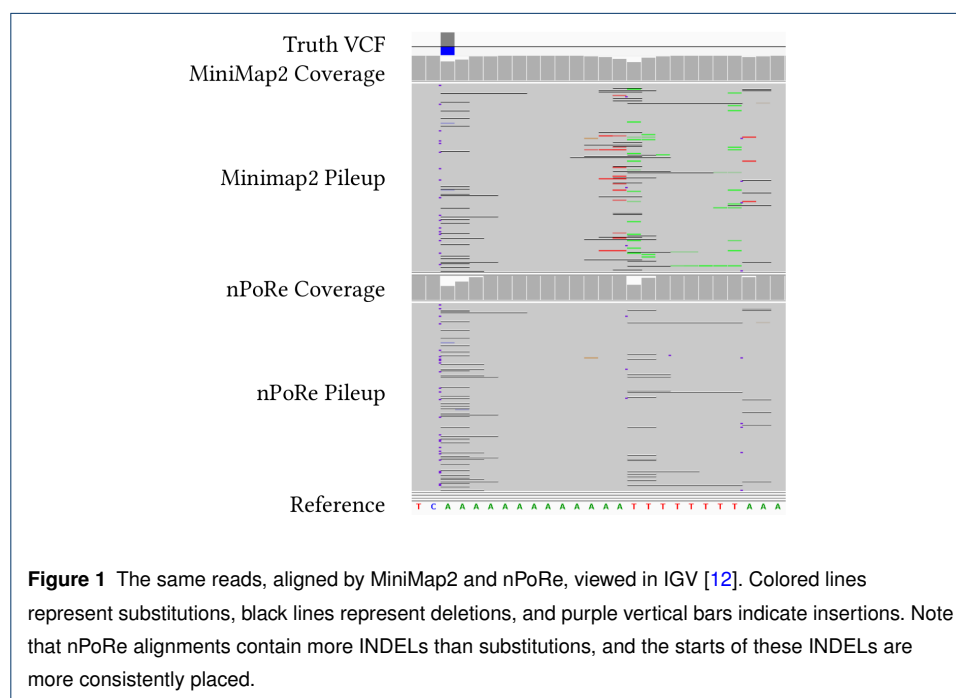
### Nanopore Variant Calling

As long read technologies have matured and basecalling accuracy has increased to over 99%, their popularity has grown accordingly [1, 2]. Long reads are essential for spanning repetitive regions and unambiguously mapping reads. Last year, the first gapless human genome sequence was constructed by the T2T consortium by combining PacBio HiFi and ONT nanopore long reads [3]. Nanopore sequencing in particular has gained popularity due to its impressive read lengths, low cost, real-time results, and direct calling of base modifications [4, 5, 6].

The two current leading nanopore variant callers are Clair3 (developed by the HKUCS Bioinformatics Algorithm Lab) and PEPPER-Margin-DeepVariant (a collaboration be-

tween UCSC and Google Health, hereafter referred to as PEPPER) [7, 8]. Both tools have converged on a similar variant calling pipeline: basecalling, read alignment, pileup-based variant calling (using pileup summary statistics), read phasing, and full-alignment variant calling (using all read information).

Despite posting impressive F1 scores ( $\geq 0.995$ ) for SNP calling, nanopore variant callers struggle with accurately identifying INDELs in low-complexity regions [8, 9, 7]. Most recent nanopore variant calling advances in this area have come from improvements in machine learning and data representation. For example, the move from prior work Clairvoyante [10] to Clair [9] involved “*an entirely different network architecture and learning tasks*”. Clair3 then split the model into a pileup caller to filter out the noise and a higher-dimensional full-alignment caller to make the more difficult decisions [7]. PEPPER examined sorting reads by haplotype and a new architecture, and DeepVariant explored numerous possible data representations for final calling [8, 11]. Orthogonally, we show that improved INDEL calling performance can be achieved through better read alignment by introducing novel gap penalties for homopolymers and tandem repeats, or “*n-polymers*”.



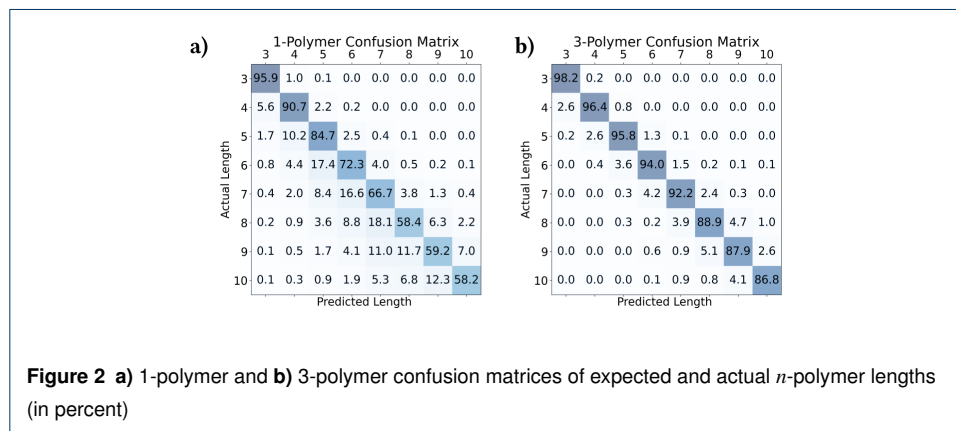
## Nanopore Read Alignment

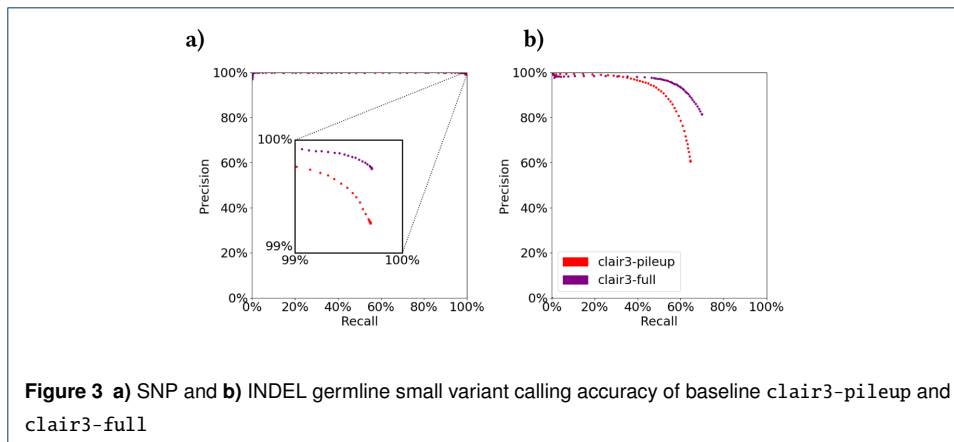
In order to maximize the accuracy of pileup-based variant calling, reads should be aligned such that actual mutations are always aligned to the same location, despite sequencing

errors. We find that simply using traditional affine gap penalties is not ideal because gap penalties  $G_{\text{open}}$  and  $G_{\text{extend}}$  are static, regardless of context [13]. For example, although our dataset consisted of only 0.8% INDEL errors, homopolymers of length 10 contained an INDEL error 41.8% of the time. Without lowering the INDEL penalty in the context of repetitive sequences, there is a mismatch between the likelihood and alignment penalty of common sequencing errors. This has an outsized impact on fine-grained read alignment, often at the expense of consistently aligning actual mutations.

Figure 1 demonstrates a specific example where static INDEL gap costs cause poor alignment concordancy in low-complexity regions. Reads are identical in the two pileups shown; only the alignments differ. In this example, two adjacent homopolymers are basecalled with inconsistent lengths. nPoRe recognizes that these two events were most likely independent, and separates them into two homopolymer length mis-calls/variants. In contrast, MiniMap2 merges two INDELs whenever possible, or aligns homopolymer length differences as SNPs when one homopolymer is lengthened and the other is shortened, resulting in inconsistent alignment. According to the truth VCF, the first homopolymer of all As had a single deletion. Looking at the third base in the coverage graphs in Figure 1, we can see that nPoRe placed a deletion here for a much larger fraction of reads than MiniMap2.

The likelihood of incorrectly basecalling an INDEL within a homopolymer increases significantly as homopolymer length increases. Figure 2a shows the confusion matrix for actual and basecalled homopolymer lengths in our dataset. This same trend is visible for tandem repeats of longer length, though to a lesser extent (Figure 2b).

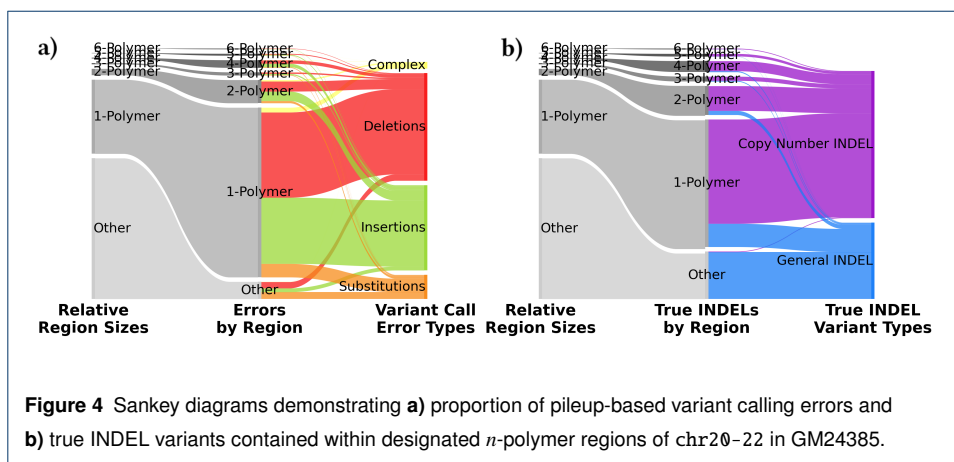




### Nanopore INDEL Accuracy

Nanopore-based variant callers have historically struggled with INDELs, particularly with recall. Although Clair3 achieves 99.67% precision and 99.60% recall for SNP variant calling, it achieves only 90.86% precision and 64.73% recall for INDELs [7]. PEPPER v4 performs similarly, with 99.61% and 99.62% SNP precision and recall but just over 90% precision and 60% recall for INDELs [8]. The most recent evaluation available shows PEPPER v7 achieving 93% precision and 76% recall for INDELs, at 85× coverage [14].

Our own evaluation confirms these findings, and furthermore attributes the loss of INDEL recall to the first pileup-based variant calling step. Figures 3a and 3b show SNP and INDEL precision recall curves, respectively, for both Clair3's pileup and full-alignment models. Note that although the more complex full-alignment model significantly improves precision, it cannot improve recall as dramatically; only variant calls and low-confidence reference calls from the previous pileup-based step are considered.



Although substitutions comprise a majority (83.75%) of the actual small germline variants in our dataset, INDELs account for 92.36% of the pileup-based false negative and 80.79% of false positive errors. Figure 4a shows that of these errors, 92.29% occur within *n*-polymer regions, despite *n*-polymer regions covering just 37.07% of evaluated regions. By improving the alignment of reads in these small *n*-polymer regions, we can have a significant impact on overall variant calling accuracy.

Ground truth INDEL mutations are over-represented in *n*-polymer regions as well (79.64% of all INDELs). This is because Short Tandem Repeat (STR) variation is a common form of mutation due to strand slippage during DNA replication, resulting in one or more copies of a repeated unit being gained or lost. We define copy number INDELs as *n*-polymers (3+ exact copies of the same repeat unit), with a differing number of copies from the expected reference. For example, AAAA→AAAAA and ATATAT→ATAT meet this definition, but ATAT→ATATAT, AATAATAAAT→AATAAT, and ATATAT→ATATA do not. Despite our relatively strict definition of *n*-polymer copy number INDELs, however, 65.82% of all INDELs met this classification (Figure 4b). nPoRe’s algorithm is directly designed to reduce alignment penalties for *n*-polymer copy number INDELs and improve alignment in low-complexity regions.

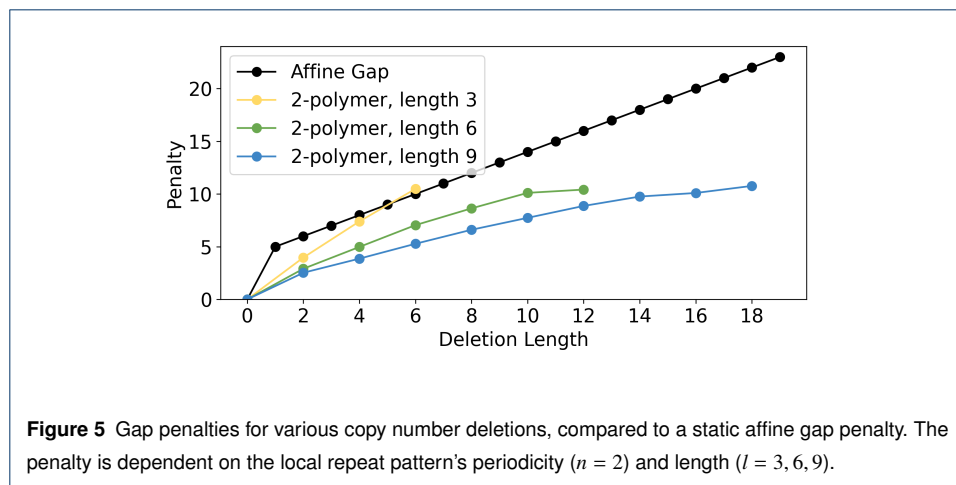
## Related Work

Variable gap penalties have been around for a long time. In 1995, Thompson first introduced per-position gap opening and extension penalties [15]. Since then, the sub-field of homologous protein sequence alignment has made extensive use of variable gap penalties (PIMA [16], FUGUE [17], and STRALIGN [18]) due to a high correlation between INDEL likelihood and the existence of protein secondary structures such as  $\alpha$ -helices and  $\beta$ -strands. SSALN was the first to use empirically-determined penalty scores (an approach similar to our own) [19], and SALIGN greatly increased the flexibility of the gap penalty function, although with a corresponding increase in computation [20]. Unfortunately, none of the numerous extensions these earlier works made to traditional Needleman-Wunsch alignment are directly applicable to the observed problem of long read *n*-polymer alignment.

Affine gap penalties belong to a larger class of “convex” gap penalties, which also includes piecewise linear and logarithmic gap penalties [21]. These more complex alternatives solve a different problem: reliably grouping several medium-sized gaps into one larger gap. They do this by decreasing the penalty for gap extension with the length of the gap,

and are commonly used for accurate alignment of large structural variants [22]. Such convex gap penalties do not solve the issue of fine-grained read alignment because they are still context-agnostic and at short INDEL lengths are highly similar to an affine gap penalty.

Several works have explored proper alignment of Short Tandem Repeats (STRs), although most function as INDEL variant callers rather than read realigners [23, 24, 25]. More recently, machine learning based approaches for final variant calling have outperformed these earlier statistical approaches [8, 11, 10, 26]. Several newer works do focus on read realignment, however. ReviSTER is one such tool for revising mis-aligned/mapped reads through reference reconstruction with local assembly, though this is primarily helpful for improving mapping, not alignment. The Broad Institute has incorporated into their standardized analysis pipeline (Genome Analysis ToolKit, or “GATK”) an IndelRealigner, recognizing that INDELs are frequently mis-called as SNPs at read edges [27]. STR-realigner is most similar to our work. It flags STR regions and aligns them separately, allowing repeated traversal of STRs during alignment [28]. They find that this approach improves the consistency of read alignment in and near repeated regions, improving downstream variant calling. STR-realigner was designed for short reads, however, and its runtime  $\Omega(n^2)$  which is perfectly fine for short reads of length 101bp is not unacceptable for long reads which regularly reach lengths upwards of 100kbp.



Our work introduces a variable gap penalty for  $n$ -polymer copy number INDELs, as shown in Figure 5. INDELs are more likely to occur in  $n$ -polymers, and so we provide a lower context-specific gap penalty, allowing only copy number INDELs. The exact sequence is not considered in this work; all 2-polymers of length 3 are scored the same (e.g. ATATAT and TGTGTG).

This work makes the following contributions:

- We identify the main source of nanopore germline small variant calling errors to be INDEL false negatives in tandem repeat and homopolymer (“*n*-polymer”) regions during pileup-based variant calling
- We show that context-agnostic affine/convex gap penalties do not accurately reflect the likelihood of nanopore sequencing errors in *n*-polymer regions
- We extend Needleman-Wunsch affine gap alignment to include context-dependent gap penalties for more accurately aligning *n*-polymers
- We introduce “follow-banding” for efficient read realignment
- We develop a VCF standardization method that ensures variants are reported in the same format as our nPoRe realigner
- We show that haplotype phasing and nPoRe realignment significantly improve pileup-based variant calling accuracy

## Results

### Overview

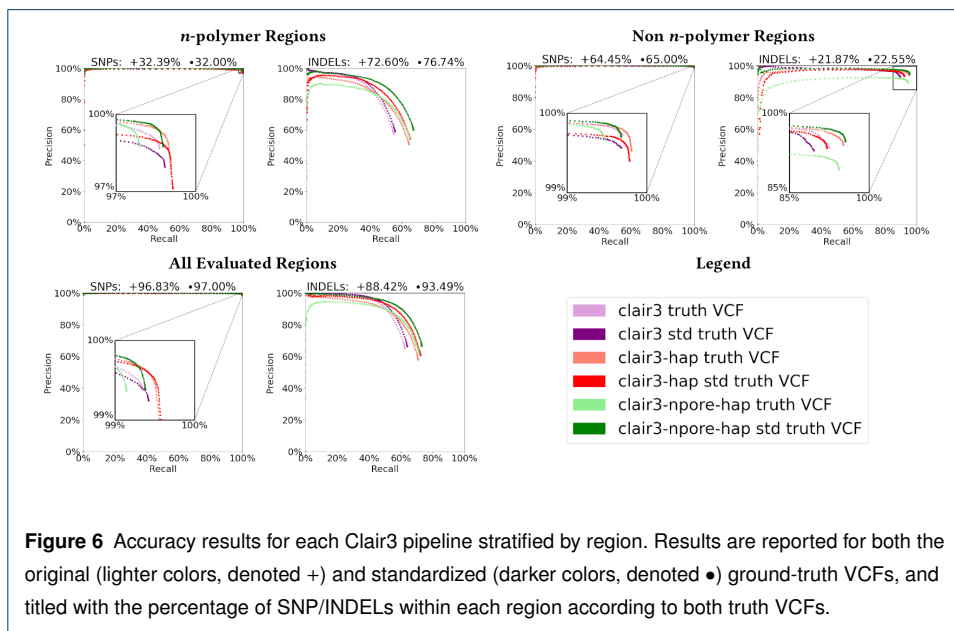
This work focuses on improving the accuracy of germline small variant calling (heritable mutations < 50bp in size). We do so by realigning mapped reads (inputting and outputting in standard BAM format) to improve fine-grained alignment and read concordance by adjusting each read’s CIGAR string. Because we are concerned only with small variants, performing realignment within a  $\pm 50$ bp window of the original mapping/alignment is sufficient. This work is independent of downstream variant caller, and nPoRe can be used in combination with either Clair3 or PEPPER. To evaluate nPoRe, we retrain Clair3 from scratch with MiniMap2- and nPoRe-realigned reads. We find that when retraining Clair3, it is beneficial to “standardize” the ground truth VCF to report variants in a manner similar to nPoRe-realigned reads (details in Methods). Realigning reads with nPoRe is relatively efficient and results in a significant increase in read concordance, which translates well to an improvement in final variant calling accuracy.

### Accuracy

Figure 6 reports the performance of all three evaluated Clair3 pipelines, with precision and recall for SNPs and INDELs given separately for each sub-region. Results are reported for both the original and standardized ground-truth VCFs (see Methods). Figure 6 shows that *n*-polymer regions are responsible for the majority of INDEL errors, since with

these regions excluded, INDEL precision and recall both exceed 95%. Performance in tandem repeat regions alone is relatively good, and homopolymers account for the majority of remaining errors. For a fixed INDEL precision of 2/3, sorting reads by haplotype (clair3→clair3-hap) improves INDEL recall from 63.76% to 70.66%. Realigning reads with nPoRe (clair3-hap→clair3-npore-hap) further improves INDEL recall to 73.04%.

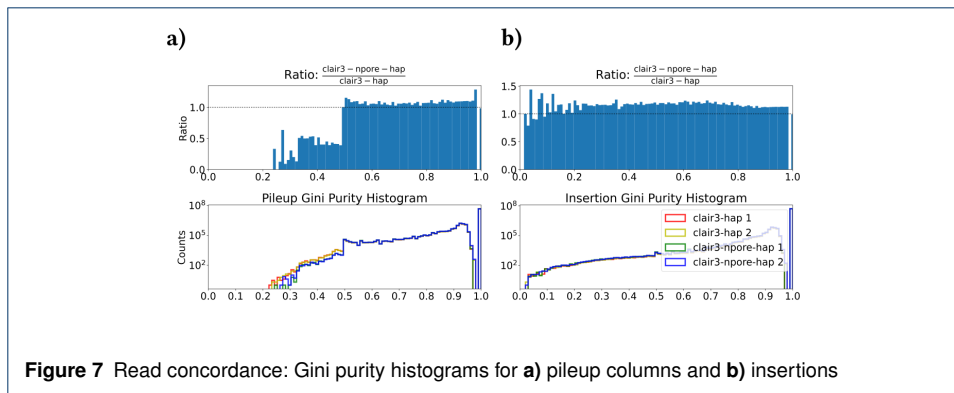
We chose to perform evaluations using both VCFs because although they contain the exact same information, the “standardized” VCF was more likely to report several INDELs instead of several SNPs (due to the lower *n*-polymer shortening/lengthening penalty), and occasionally broke an INDEL up into several smaller INDELs. As a result, the standardized VCF had 18.05% more INDELs (31,104) and 1.45% fewer SNPs (155,163) than the original VCF (25,500 INDELs and 157,454 SNPs). hap.py’s vcfeval engine assigned partial credit for SNPs less frequently to nPoRe-aligned reads. The standardized VCF resulted in apparent higher INDEL recall for all variant callers, due to the increase in total INDELs.



## Read Concordance

If sequenced reads were to not contain errors, they would all perfectly agree with one another and variant calling would be easy. We would like to maximize the extent to which reads agree with one another, which we term “concordance” and measure per-haplotype and per-position in terms of Gini purity. Gini purity is defined as  $GP = \sum_{i=1}^N \mathbb{P}(i)^2$ , where





$N$  is the number of classes and  $\mathbb{P}(i)$  is the probability of class  $i$ . Figure 7a (lower graph) shows the resulting Gini purity histogram with the classes A, C, G, T, - (deletion) on a logarithmic y-scale. If all reads agree,  $GP = 1$ . If 50% call T and 50% call C,  $GP = 0.5$ . In the worst case, where there is an even split between the five classes,  $GP = 0.2$ . Reference positions with low Gini purity scores are therefore difficult to call, and are a likely source of both false positive and false negative variants. The lower graph in Figure 7 compares the Gini purity score distributions in MiniMap2 and nPoRealigned BAMs. It shows a marked  $\approx 50\%$  decrease in positions with Gini purity less than 0.5 for the nPoRe-realigned BAM, demonstrating that nPoRe greatly improves alignment concordance across reads in difficult regions.

Read concordance in the phased BAM pileup, evaluated by Gini purity computed per reference position, is shown in Figure 7a. Insertion concordancy was evaluated separately, in Figure 7b, where the classes are all insertions between base  $k$  and  $k + 1$  (e.g.  $\epsilon, A, AA, AAA, AT, ATT \dots$ ). We plot insertions separately because the variable number of classes greatly affects the Gini purity score distribution. There appears to be an approximately 10% increase for all imperfect Gini purity scores, which we attribute to nPoRe's increased likelihood of calling INDELs (and as a result, more average classes and greater divergence).

### Timing

We performed our evaluations on a system with 2× Intel Xeon E5 2697v3 2600MHz CPUs and 64GB total RAM. Timing results are shown in Table 1. From this evaluation, it is clear that any pipeline stages requiring computation on the full BAM file (marked with \*) are considerably more expensive than working with just putative variants, a small fraction of the entire genome. Although our nPoRe realigner accounted for 79.6% of total CPU time,

	Step	Real Time	CPU Time
	*align reads	1,218:01	7,808:24
	generate tensors	44:29	301:53
	train <code>clair3</code>	38:18	54:22
	call variants	86:26	2,392:17
	phase variants	347:58	344:05
	*phase reads	240:32	228:03
	*index BAM	1,138:09	1,750:13
	phase truth VCF	364:23	360:03
	standardize truth VCF	546:31	3,756:46
	*realign reads	2,168:15	111,792:55
	*generate haplotype tensors	1,363:23	3,162:48
	train model	41:40	66:29
	call variants	200:08	8,343:01

**Table 1** Timing results for stages in the `clair3-npore-hap` pipeline (Table 3).

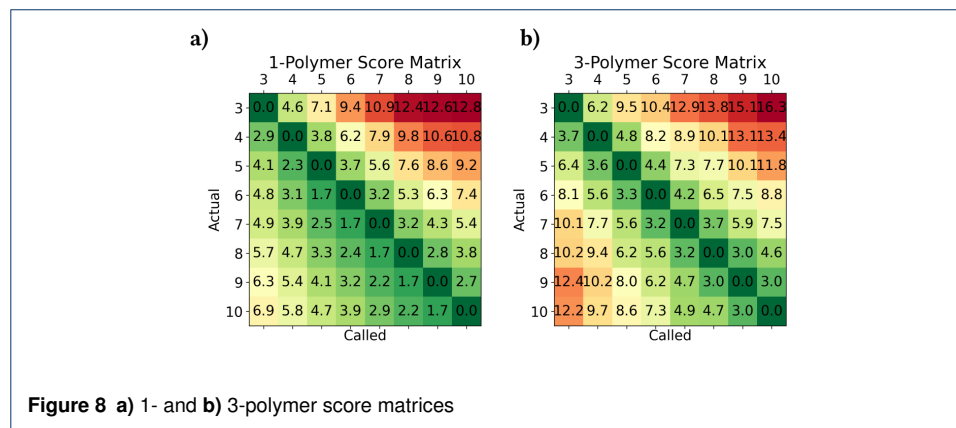


**Figure 8** a) 1- and b) 3-polymer score matrices

it only accounted for 27.8% of the real runtime, or just under twice as long as it took to index the BAM. nPoRe's CPU time was 51.6× its real time on our system with 56 total cores, demonstrating that we took full advantage of the available parallelism.

### Score Matrices

Figure 8 shows the calculated score matrices for 1- and 3-polymers, corresponding to the confusion matrices in Figure 2. In general,  $n$ -polymer INDELs are penalized less than the general-case affine gap INDEL penalty. Additionally, insertions are more common than deletions, and INDELs are more common in  $n$ -polymers of shorter repeat unit length ( $n$ ).

## Discussion

The current nPoRe algorithm implementation was designed to demonstrate that there is a significant difference in INDEL rates between repetitive and non-repetitive sequences, due

to the common occurrence of  $n$ -polymer copy number INDELs and sequencing errors. In order to do so, we decided upon a strict definition of  $n$ -polymers that requires at least three repetitions of the exact same repeat unit. We found that this strict definition includes around 65% of all INDELs in our dataset. Despite this, there are many repetitive regions in which sequencing errors are common but do not meet our strict definition of an  $n$ -polymer. For example, the sequence AAATAAAATAAATAAAT is not an  $n$ -polymer because the second repetition of AAAT has an additional A. A more lenient definition of  $n$ -polymers would result in a broader application of reduced INDEL gap penalties for repetitive regions and may improve alignment results further. Additional leniency, however, would come at the cost of increased computation. Alternatively, we could consider the actual  $n$ -polymer sequence (instead of just unit size  $n$  and length  $l$ ) during alignment, which would also increase computation and memory requirements.

We find alignment speed to be the greatest practical limitation of our nPoRe aligner, despite writing our alignment kernel in Cython and taking full advantage of the available parallelism. Genomics datasets are inherently large, and a hyper-optimized implementation with SIMD intrinsics and reduced data width may be necessary for large-scale applications. We have already explored reducing memory usage by shifting to a difference-based  $n$ -polymer cost matrix and only storing  $2 * n_{\max} + 1$  matrix rows in memory, resulting in about 10-20% performance gains. Replacing the  $n$ -polymer cost matrix with a best-fit surface or function would likely improve efficiency further by reducing irregular memory accesses. We consider the main contribution of this work to be identifying fine-grained alignment as a significant source of small variant calling INDEL errors and developing an algorithmic solution. Speed can be improved through further engineering efforts.

The current design of nPoRe operates under the principles of reference-guided alignment and considers each read independently, using aggregate statistics on INDEL likelihood to better estimate the most likely alignment of each read. A promising avenue for future work, however, would be to consider the alignments of all reads overlapping the same reference location simultaneously, and select the most likely alignment in the context of other overlapping/neighbors alignments. Consensus graph-based alignments can take additional local information (provided by other overlapping reads) into account in order to provide more consistent alignments between reads.

The astute reader may notice that our  $n$ -polymer copy number INDEL penalties were calculated based on the measured negative log likelihood of occurrence in the original BAM,

which as we've pointed out, has issues with fine-grained alignment. Does that mean that nPoRe's gap penalties are entirely wrong? Not really. The original BAM's fine-grained alignment is inconsistent across reads, since alignments are unduly affected by nearby errors. Even if this were to affect our estimate of  $n$ -polymer copy number INDEL likelihoods by  $2\times$ , the effect on INDEL penalty is only  $\log 2 \approx 0.69$ . Figure 8 shows that for a 3-polymer, the penalty for a 3-base deletion ranges from 3.7 to 3.0 as length increases from 3 to 10. Since MiniMap2 is biased against  $n$ -polymer INDELs, we are only underestimating likelihood and the  $n$ -polymer penalties should all be slightly lower (by  $< 0.5$ ). In contrast, without these  $n$ -polymer INDEL scores, a 3-base deletion is penalized  $G_{\text{open}} + 2 * G_{\text{extend}} = 7$ . Our algorithm successfully compensates for the orders of magnitude increase in likelihood of INDELs in  $n$ -polymer regions. A second iteration of INDEL likelihood estimation using the nPoRe-realigned BAM would further improve score estimation.

## Conclusions

We identify the main source of nanopore germline small variant calling errors to be copy number INDEL false negatives in  $n$ -polymer regions, and show that context-agnostic affine gap penalties do not accurately reflect the likelihood of nanopore sequencing errors. To improve nanopore pileup-based variant calling accuracy, we explore correcting fine-grained read alignment. This work extends Needleman-Wunsch affine gap alignment to include repeat-aware gap penalties for  $n$ -polymers. In doing so, we also develop “follow-banding” for efficient long read realignment and a method for standardizing ground-truth VCFs. We demonstrate that read realignment improves read concordance and variant calling accuracy, and release nPoRe<sup>[1]</sup> as an open source tool.

Despite being located in low-complexity regions, calling the length of tandem repeats is clinically relevant. There is an entire class of neuropathological disorders associated with copy number variation known as “Tandem Repeat Disorders”, or TRDs. Huntington's Disease is one such disorder caused by 40 or more repeats of the CAG 3-polymer at the end of the gene *HTT*, instead of a normal 10-30 copies. Other TRDs include Fragile X Syndrome, Kennedy's Disease, myotonic dystrophy, and several spinocerebellar ataxias [29]. Since nPoRe significantly improves read alignment and variant calling in tandem repeat regions, it will lead directly to more accurate diagnoses of such disorders.

---

<sup>[1]</sup><https://github.com/TimD1/nPoRe>

## Methods

### Overview

Because we have designed a read **realignment** algorithm, we trust the initial mapping of each read. Each read and its corresponding section of the reference genome are realigned, and a new traceback (alignment path) is computed. In other words, our solution simply adjusts the CIGAR string of each read within the input BAM file to better model the most likely mutations and sequencing errors in an effort to achieve greater concordancy between reads.

Our realignment algorithm is an extension of the Needleman-Wunsch algorithm for global alignment [30]. In addition to including known improvements such as an affine gap penalty and custom substitution penalty matrix [31], our algorithm allows the shortening and lengthening of homopolymers and tandem repeats (i.e. ACACAC→ACACACAC).

### *n*-Polymer Repeats

The literature often categorizes sequences consisting of one repeated base as “homopolymers”, and repeated sequences of at least two bases as “tandem repeats” or “copolymers” [8, 32]. Short tandem repeats (STRs) are often defined as repeated units 2-6 bases in length, and are also known as “microsatellites” or “simple sequence repeats” (SSRs) [33]. Rather than treating these classifications separately for nPoRe, **we define an *n*-polymer to consist of at least 3 exact repeats of the same repeated sequence, where the repeat unit is of length 1 to 6 bases** ( $1 \leq n \leq 6, l \geq 3$ ). For example, homopolymers such as AAAAA ( $n = 1$ ) and tandem repeats such as ACACACAC ( $n = 2$ ) and TTGTTGTTG ( $n = 3$ ) are *n*-polymers. Shorter or irregular repeated sequences such as AATTAATT and ACAACAAACAC are not.

An upper threshold of  $n_{\max} = 6$  was selected because there is a marked decrease in the frequency of *n*-polymers for  $n > 6$ . Tandem repeats are usually defined with the same upper bound on repeat unit length *n* for the same reason. Figure 4 shows that 6-polymers are already uncommon. Furthermore, nanopore R9.4.1 sequencers fail to accurately call the length of *n*-polymers because the pore’s effective sensing width is 5-6 bases; i.e. the measured signal depends upon 5-6 adjacent bases simultaneously [34]. An *n*-polymer for  $n \leq 6$  is usually observed as a nearly-constant signal due to exact repetition, from which it is difficult to determine repeat length. For *n*-polymers where  $n > 6$ , this is less of a problem, and fewer errors are observed. For a similar reason, a minimum *n*-polymer length of  $l = 3$

was decided upon to classify a repeated sequence as an  $n$ -polymer. If  $l = 2$ , there is never a series of  $n$  bases bordered on both sides by another copy of the same  $n$  bases. The two copies of  $n$  bases are each adjacent to a non-repeating region, and as a result the measured signal is non-constant and few basecalling errors occur.

### Penalty Functions

For each read, differences from the reference genome can be attributed to either sequencing errors or actual mutations. Regardless of origin (error or mutation), our goal is to align these reads to the reference in a manner that accurately captures the change that occurred. Existing aligners fail to do this by defining substitution and gap penalties based on estimated rather than measured rates of occurrence, and the algorithms do not account for common sequencing error modes such as tandem repeat length errors in nanopore sequencers. In contrast, we calculate penalties based on frequency measurements from the input BAM file. We define the penalty score for each difference (whether error or mutation) to be the negative log likelihood of that event occurring. As a result, finding the minimum-penalty alignment path is equivalent to finding the most likely set of errors and mutations that have occurred (assuming independence).

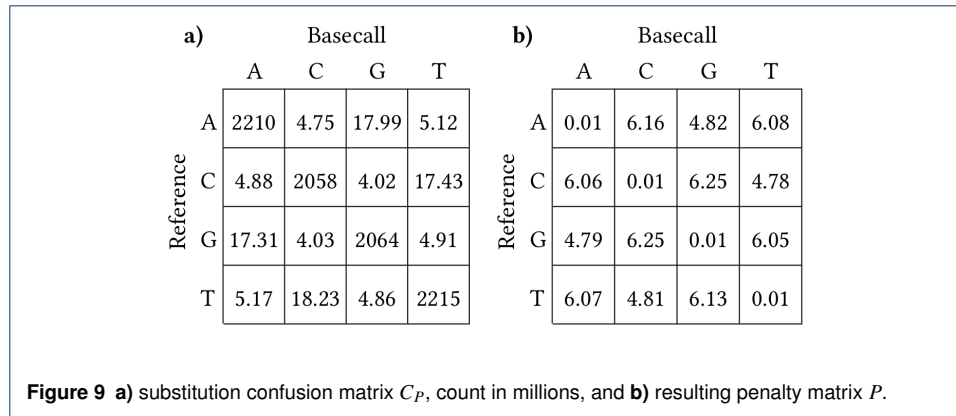
### Substitution Penalty Matrix

Figure 9 shows the calculation of substitution penalty matrix  $P$  from confusion matrix  $C_P$ , using Equation 1.  $\epsilon = 0.01$  was included for numerical stability in the case that certain events were never observed. If we consider bases  $x = \text{"ACGT"}$ , then  $P[i, j]$  is the negative log probability that base  $x[i]$  was observed as base  $x[j]$ , either through a mutation or sequencing error:

$$P[i, j] \approx -\log \mathbb{P}(x[i] \rightarrow x[j]) \approx -\log \frac{C_P[i, j] + \epsilon}{\text{sum}(C_P[i, :]) + \epsilon} \quad (1)$$

### Affine Gap Penalties

Confusion matrices for insertions ( $C_I$ ) and deletions ( $C_D$ ) were first generated by measuring the occurrence of small INDELs in the input BAM. Both matrices are 1D, since the expected INDEL length is always zero. Then, penalties were calculated by determining the negative log probability of each INDEL length  $i$  occurring:  $-\log \frac{C_I[i] + \epsilon}{\text{sum}(C_I) + \epsilon}$ . From these penalties, a best-fit gap opening penalty  $G_{\text{open}}$  of 5 and gap extension penalty  $G_{\text{extend}}$  of 1 was selected for both insertions and deletions [31].



### Tandem Repeat Penalty Matrix

First, confusion matrix  $C_N$  of shape  $6 \times 100 \times 100$  was generated by comparing expected and observed  $n$ -polymer lengths  $l$  (up to 100). For each  $n$ , or repeat unit size 1–6, a penalty matrix was calculated using the following equation, where  $i$  is the expected repeat length and  $j$  is the measured repeat length.

$$N[n, i, j] \approx -\log \mathbb{P}(n, i, j) \approx -\log \frac{C_N[n, i, j] + \epsilon}{\text{sum}(C_N[n, i, :]) + \epsilon}$$

To improve penalty regularity, particularly for longer  $n$ -polymers where few examples were observed, the following two properties were enforced for each possible combination of  $k > 0, n, i$  within the bounds of  $N$ :

- shorter INDELs are more likely:

$$N[n, i, i \pm k] > N[n, i, i \pm (k + 1)]$$

- longer  $n$ -polymers are more likely to contain an INDEL of a given size:

$$N[n, i + 1, (i + 1) \pm k] > N[n, i, i \pm k]$$

### Reference Annotation

Reference annotations are used to track eligible  $n$ -polymers during alignment. For each possible  $n$ -polymer repeat unit length from  $n = 1$  to  $n_{\max}$ , each reference position is annotated with  $l$ , the length or number of consecutive repeat units, and  $idx$ , the 0-based index of the current repeat unit ( $0 \leq idx < l$ ). Table 2 shows example annotations for a short reference sequence for  $n = 1$  and  $n = 2$ . Recall that in order for a sub-sequence to be considered an  $n$ -polymer, the pattern must repeat exactly at least three times. Annotations may overlap, and non-zero annotations are only placed at the start of every  $n$ -polymer repeat unit.

Reference: A T A T A T A T T T T T A A A G C G C G C	
n=1	<i>l</i> : 0 0 0 0 0 0 0 5 5 5 5 3 3 3 0 0 0 0 0
	<i>idx</i> : 0 0 0 0 0 0 0 0 1 2 3 4 0 1 2 0 0 0 0 0
n=2	<i>l</i> : 4 3 4 3 4 3 4 0 0 0 0 0 0 0 3 0 3 0 3 0
	<i>idx</i> : 0 0 1 1 2 2 3 0 0 0 0 0 0 0 0 0 1 0 2 0

**Table 2** Example  $n$ -polymer reference annotations

### Alignment

Before aligning read  $r$  to reference  $R$ , the reference is annotated with  $n$ -polymer information as discussed previously. Then, the five matrices  $D, I, M, S$ , and  $L$  are computed in lockstep one cell at a time, in that order. These matrices of size  $|r| \times |R|$  represent the states Deleting, Inserting, Matching, Shortening  $n$ -polymers, and Lengthening  $n$ -polymers, respectively. For each cell, each matrix stores a tuple  $(val, pred, run)$  containing the accumulated penalty *value*, in addition to the *predecessor* matrix and consecutive movements (*run*) within that matrix for backtracking purposes.

Figure 10 demonstrates the cell dependency patterns and penalties in greater detail. For example, when computing cell  $i, j$  in  $S$ , the reference annotations  $l$  and  $idx$ , are first retrieved for each  $n$  for  $R[j]$ . All dependencies (marked with  $\bullet$  for  $S$ ) in Figure 10 are considered, and the minimum value of these dependencies' cell values plus the associated penalties is calculated and stored in the result cell (marked with  $\bullet$  for  $S$ ). In other words, when looking at  $S[i, j]$ , for each  $n$ , we do:

$$S[i, j + n] = \min(M[i, j] + N[n, l, l - 1],$$

$$S[i, j - run] + N[n, l, l - 1 - run/n])$$

These two movements correspond to starting to shorten a tandem repeat (state  $M \rightarrow S$ ), and continuing to shorten a tandem repeat (state  $S \rightarrow S$ ). All movements into matrices  $S$  and  $L$  such as these are only allowed conditionally based on reference annotations (described in the following section). Note that if matrices  $S\bullet$  and  $L\blacktriangle$  are omitted (as well as all  $\bullet$  and  $\blacktriangle$  dependencies), this algorithm is equivalent to Needleman-Wunsch alignment with an affine gap penalty [30].

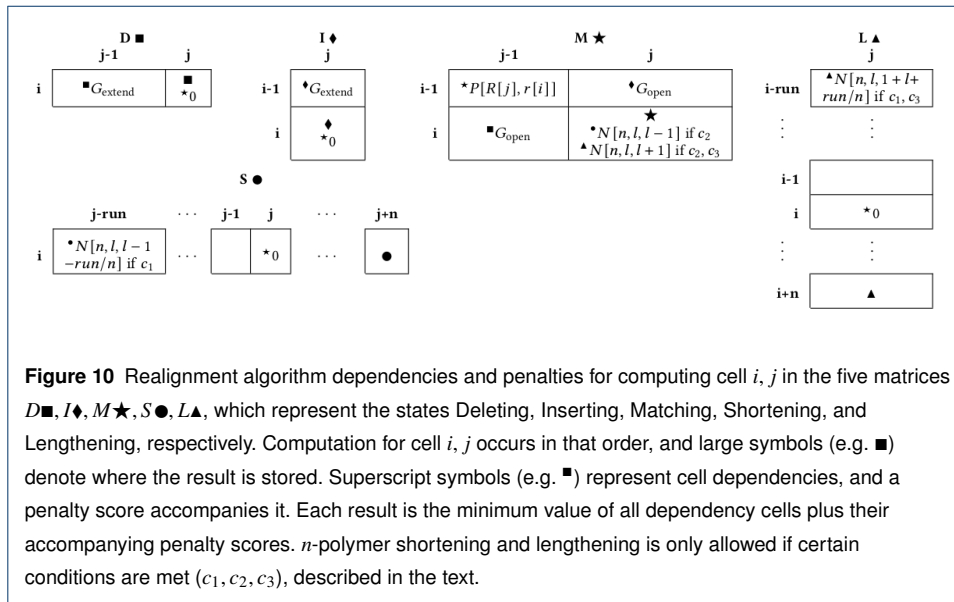
### $n$ -Polymer INDEL Conditions

Unlike matrices  $D, I$ , and  $M$ , the results for matrices  $S$  and  $L$  are stored several cells ahead of the current cell, and cell dependencies are only allowed conditionally based on the refer-



ence annotations. This ensures that matrices  $S$  and  $L$  only allow INDELs which change the copy number of tandem repeats and homopolymers. Here are the three conditions  $c_1, c_2, c_3$  used by our algorithm, and referenced in Figure 10:

$$\begin{aligned}
 c_1 &= l > 0 && \text{start of repeat unit} \\
 c_2 &= l > 0 \text{ and } idx == 0 && \text{start of } n\text{-polymer} \\
 c_3 &= R[j+1 : j+1+n] == \\
 &\quad r[i+1 : i+1+n] && \text{next } n \text{ bases of } r \text{ match } R
 \end{aligned}$$



## Backtracking

Traceback occurs entirely within matrix  $M$ , and relies on *predecessor* and *run* length information computed during the forward pass. The selected optimal alignment path is computed by Algorithm 1 and reported in the output BAM file in the form of a CIGAR string. CIGAR strings are composed of the symbols M, I, and D. Reference Matches, Insertions, and Deletions, correspond to diagonal, vertical, and horizontal movements in the alignment matrix, respectively. An example alignment is denoted by  $\bullet$  in Figure 11a. After computation, the computed CIGAR string is collapsed ( $\text{MMMDIMMM} \rightarrow 3\text{M1D1M1I2M}$ ).

## Follow-Banding

As mentioned previously, the primary goal of our read realignment algorithm is to more accurately model the mutations and sequencing errors in fine-grained alignment. Therefore, we can skip read mapping and trust the read start position reported by the previous aligner.

**Algorithm 1** Backtracking algorithm

---

```

i, j ← |r| − 1, |R| − 1
cigar ← ""
while i > 0 or j > 0 do
  (val, pred, run) ← M[i, j]
  if pred == M then
    if r[i] == R[j] then
      cigar += " = "
      i, j ← i − 1, j − 1
    else
      cigar += "X"
      i, j ← i − 1, j − 1
    end if
  else if pred == I or pred == L then
    cigar += "I" * run
    i ← i − run
  else if pred == D or pred == S then
    cigar += "D" * run
    j ← j − run
  end if
end while
return cigar[::-1]

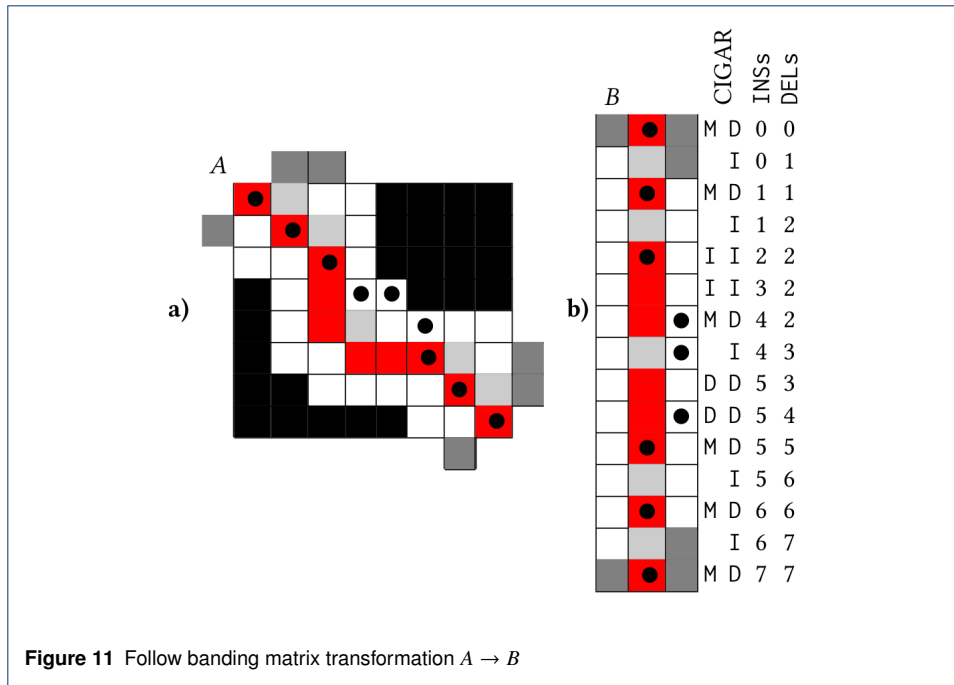
```

---

In addition to the mapping POSition field, the SAM/BAM file format [35] includes TLEN, or the template (reference) length which corresponds to the aligned read. Thus, we can align read  $r$  to a small subsection of the reference  $R[\text{POS} : \text{POS} + \text{TLEN}]$ . Barring any large INDELs,  $\text{TLEN} \approx |r|$ , and we transform our alignment problem from  $O(|R||r|)$  to  $O(|r|^2)$ .

Moreover, we can use the SAM/BAM file's existing CIGAR string to simplify our alignment problem even further. Our optimal alignment will likely follow a path close to that of the original alignment. Figure 11a demonstrates how we can compute the alignment matrix (new optimal path denoted by  $\bullet$ ) in a narrow band  $b = 1$  that follows the original alignment (red cells). Dark gray and black cells are not computed. Essentially, we use the CIGAR string to precompute the movement directions for adaptive banded alignment as proposed by Suzuki and Kasahara [36], instead of using a heuristic comparing penalty scores on the band's edge.

Firstly, all M CIGAR operations are converted to ID, an insertion followed by a deletion. This change is shown in Figure 11, supplementing the original red alignment path with light gray cells. Next, computation proceeds one anti-diagonal row of width  $2b + 1$  at a time, centered on the alignment path. The computation of anti-diagonal rows shifts either right or downward at each step, governed by the previous CIGAR operation, D or I. These anti-diagonal rows can be stored efficiently in matrix format, as demonstrated in Figure 11b.



Transforming the banded  $|r| \times |r|$  matrix  $A$  to a  $(2b + 1) \times 2|r|$  matrix  $B$  saves significant space because nanopore sequencing read lengths  $|r|$  can be up to several million bases [4], while realignment works well with a band width of  $b = 30$ .

Offset arrays INSSs and DELs can be precomputed using the CIGAR (Figure 11). Given a cell in matrix  $B$  with indices  $i, j$ , its position in matrix  $A$  can be computed using the following formula:

$$\text{row} = \text{INSS}[i] + b - j \quad \text{col} = \text{DELS}[i] - b + j$$

### Time and Space Complexity

#### Reference annotations

The worst-case time complexity for computing the reference annotations is  $O(|R|n_{\max}^2 l_{\max})$ , where  $|R|$  is the length of the reference  $R$ , and  $n_{\max}$  is the maximum  $n$ -polymer considered, and  $l_{\max}$  is the maximum  $n$ -polymer length. Since our  $n$ -polymer score matrix  $N$  is of size  $(6, 100, 100)$ ,  $n_{\max} = 6$ , and  $l_{\max} = 100$ . Thus, the time complexity is effectively  $O(|R|)$ . Furthermore, these annotations must only be computed once, and cost can be amortized over all the reads that are aligned to the reference. We found the time required for reference annotations to be insignificant compared to alignment. These annotations require  $O(|R|n_{\max})$  space.

### Read alignment

Once the reference annotations and score matrices have been computed, the nPoRe algorithm requires  $O(|R||r|)$  time for each read  $r$ . The only additional overhead nPoRe incurs over Needleman-Wunsch with affine gaps is computing five Dynamic Programming (DP) matrices instead of three, as well as computing the new cell dependencies. All new penalties are conditional  $O(1)$  lookups. As discussed earlier, follow-banding further reduces both the time and space complexity of alignment from  $O(|R||r|)$  to  $O(b|r|)$ , where  $b$  is the band width. In total, the cost of aligning all reads is  $O(\sum_{i=1}^m b \times |r_i|)$ , where  $m$  is the number of reads, or equivalently  $O(db|R|)$ , where  $d$  is the average depth of coverage.

All our code is open source and readily available at: <https://github.com/TimD1/nPoRe>.

### Datasets

#### Reference

We used the GrCh38 reference from the Genome-In-A-Bottle (GIAB) consortium [32].

#### Reads

We obtained our FASTQ files from *ONT Open Datasets'* May 2021 re-basecalling of HG002 PromethION R9.4.1 data using Guppy 5.0.6. Specifically, we used flow cell PAG07162, prepared using the Short Read Eliminator (SRE) protocol [37]. Depth of coverage was approximately 60×. For training, we used chr1-chr19, and for testing we used chr20-chr22.

### Stratification Regions

Stratification BED regions were calculated for  $n = 1 \dots n_{\max}$  using the definition of  $n$ -polymers provided previously. Regions were extended by a single base on each side (slop=1) to include variants occurring at the edges of  $n$ -polymer regions. These BEDS were then merged and complemented as necessary to create stratification BEDS for all  $n$ -polymer regions and non  $n$ -polymer regions.

### Pipeline

The full training and evaluation pipelines for all three Clair3 configurations tested are shown in Table 3. We used minimap2 version 2.17-r954-dirty [38], clair3 version v0.1-r9 [7], whatshap version 1.0 [39], and hap.py version v0.3.14 [32]. All three

Step	clair3	clair3-hap	clair3-npore-hap	Program
align reads	✓	✓	✓	minimap2
generate tensors	✓	✓	✓	clair3/CTP.py
train clair3	✓	✓	✓	clair3/Train.py
call variants	✓	✓	✓	clair3/run_clair3.sh
phase variants		✓	✓	whatshap phase
phase reads		✓	✓	whatshap haplotag
phase truth VCF		✓	✓	whatshap phase
standardize truth VCF			✓	nPoRe/standardize_vcf.py
realign reads			✓	nPoRe/realign.py
generate haplotype tensors		✓	✓	clair3-hap/CTPHaps.py
train model		✓	✓	clair3-hap/Train.py
call variants		✓	✓	clair3-hap/run_clair3.sh
evaluate variants	✓	✓	✓	hap.py

**Table 3** Clair3 training and evaluation pipelines.

variant callers were trained from scratch using our 60× HG002 dataset on MiniMap2-aligned reads for chr1–chr19, and tested on chr20–chr22. We first extended the retrained Clair3 baseline (clair3), phasing the input reads by haplotype and training a phased pileup candidate caller (clair3-hap). This was done because it significantly improves read concordancy, and leaving reads unphased when calling difficult single-haplotype variants might overshadow concordancy improvements gained by nPoRe’s alignment algorithm. This second baseline enables us to clearly delineate the gains from haplotype phasing and our nPoRe alignment algorithm. The final configuration was clair3-npore-hap, in which we performed ordinary variant calling with clair3, phased reads by haplotype, and then realigned them with nPoRe prior to variant calling.

### Haplotype Phasing

In order to add haplotype phasing information to Clair3, a single iteration of the ordinary pileup-based pipeline was first run. Proposed variants were then phased using whatshap phase, and reads were tagged by haplotype using whatshap haplotag. We then sorted reads by haplotype into three separate BAM files. When generating the input pileup tensor for training clair3-hap and clair3-npore-hap, for each position a pileup tensor was generated for both unphased reads, reads from the first haplotype, and reads from the

second haplotype. These three pileup tensors were then concatenated to create a new input tensor for Clair3.

Truth VCF Standardization

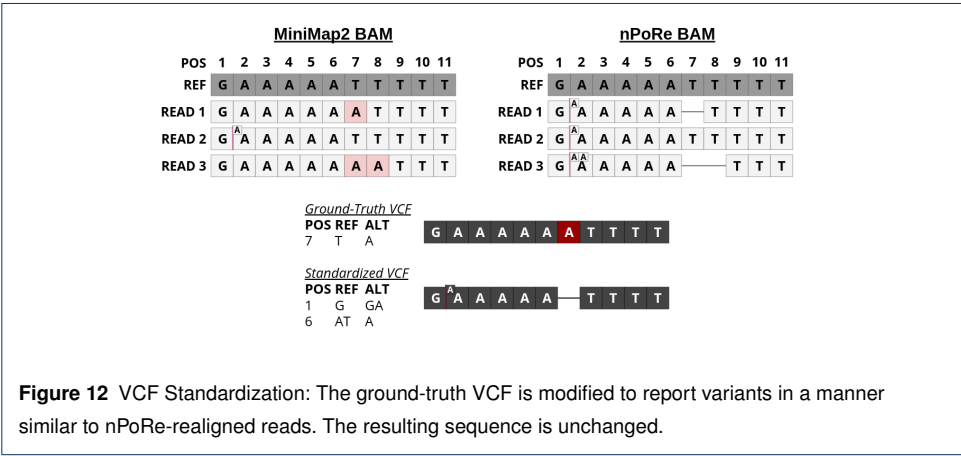


Figure 12 shows a simplified example of a typical MiniMap2 input BAM in comparison to the nPoRe-realigned output BAM. nPoRe is comparatively more likely to call *n*-polymer INDELs than SNPs, due to the reduced INDEL penalty. We found that `clair3-npore-hap` variant calling performance suffers if we train Clair3 with the original ground-truth VCF, since the realigned reads tend to report variants using an INDEL-heavy representation. To mitigate this, we altered the ground-truth VCF so that it reports variants using the same representation our aligner tends towards. An example of this “standardized” VCF is shown in Figure 12.

To achieve this, we copied our reference FASTA to create two haplotype FASTAs, and applied the phased ground-truth variants to each haplotype FASTA, storing the new CIGAR. Using a mapping position of 0, the generated haplotype references, and associated CIGARs, we considered these ground-truth haplotype references to be reads and aligned them to the original reference using nPoRe. Any substitutions, insertions, or deletions in the resulting alignment were then parsed into a new standardized ground-truth VCF file. This process ensures that the new “standardized” truth VCF contains the same exact ground-truth sequence as the original VCF when applied to the reference FASTA, but reports variants in a manner consistent with nPoRe.

## Declarations

### Ethics approval and consent to participate

Not applicable.

### Consent for publication

Not applicable.

### Availability of data and materials

The FASTQ dataset supporting the conclusions of this article is available in the [ONT Open Datasets](#) repository.

For chromosomes N = 1 to 22, we downloaded: [s3://ont-open-data/gm24385\\_2020.11/analysis/r9.4.1/20201026\\_1644\\_2-E5-H5\\_PAG07162\\_d7f262d5/guppy.v4.0.11\\_r9.4.1\\_hac\\_prom/align\\_unfiltered/chrN/guppy.v5.0.6\\_r9.4.1\\_sup\\_prom/basecalls.fastq.gz](s3://ont-open-data/gm24385_2020.11/analysis/r9.4.1/20201026_1644_2-E5-H5_PAG07162_d7f262d5/guppy.v4.0.11_r9.4.1_hac_prom/align_unfiltered/chrN/guppy.v5.0.6_r9.4.1_sup_prom/basecalls.fastq.gz).

Specifically, we used flow cell PAG07162 from the May 2021 re-baserecalling of HG002 PromethION R9.4.1 data using Guppy 5.0.6; more details regarding this data can be found [here](#).

We used the GrCh38 reference FASTA from the Genome-In-A-Bottle (GIAB) consortium [32], also made available through ONT Open Datasets:

[s3://ont-open-data/gm24385\\_2020.09/config/ref/GCA\\_000001405.15\\_GRCh38\\_no.alt.analysis.set.fasta](s3://ont-open-data/gm24385_2020.09/config/ref/GCA_000001405.15_GRCh38_no.alt.analysis.set.fasta).

The ground truth VCF and BED files were provided by GIAB at the following link: <https://ftp-trace.ncbi.nlm.nih.gov/ReferenceSamples/giab/release/AshkenazimTrio/HG002.NA24385.son/NISTv4.1/GRCh38/>.

The source code for nPoRe is available at <https://github.com/timd1/npore>, and archived through Zenodo: <https://zenodo.org/record/6260902>. nPoRe is written in Python/Cython and is available cross-platform through a public Docker container (<https://hub.docker.com/r/timd1/npore>) under the [GNU GPLv3](#) license.

### Competing interests

The authors declare that they have no competing interests.

### Funding

This project was supported by the Kahn Foundation and the National Science Foundation. The NSF supported this work under NSF Grant 2030454 and NSF Graduate Research Fellowship 1841052. Any opinion, findings, and conclusions or recommendations expressed in this material are those of the authors and do not necessarily reflect the views of the National Science Foundation.

### Authors' contributions

TD was responsible for designing and implementing nPoRe, and all subsequent data analysis. DB, RD, and SN provided valuable guidance and feedback along the way, and assisted with writing the manuscript. All authors read and approved the final manuscript.

### Acknowledgements

Although the origins of the code are now unrecognizable, it began as a fork of [swalign](#), developed by Marcus Breese.

### Author details

University of Michigan, Ann Arbor, USA.

### References

1. Lang D, Zhang S, Ren P, Liang F, Sun Z, Meng G, et al. Comparison of the two up-to-date sequencing technologies for genome assembly: HiFi reads of Pacific Biosciences Sequel II system and ultralong reads of Oxford Nanopore. *GigaScience*. 2020 12;9(12). Giga123. Available from: <https://doi.org/10.1093/gigascience/giaa123>.
2. Brown C. Technology Update; 2021. Nanopore Community Meeting. Available from: <https://nanoporetech.com/resource-centre/clive-brown-ncm-update-2021>.
3. Nurk S, Koren S, Rhie A, Rautiainen M, Bizikadze AV, Mikheenko A, et al. The complete sequence of a human genome. *bioRxiv*. 2021; Available from: <https://www.biorxiv.org/content/early/2021/05/27/2021.05.26.445798>.
4. Kilburn D, Burke J, Fedak R, Olsen H, Jain M, Miga K, et al.. High Data Throughput and Low Cost Ultra Long Nanopore Sequencing;. Available from: [https://15a13b02-7dac-4315-baa5-b3ced1ea969d.filesusr.com/ugd/5518db\\_164bac27f4654b1f94d3472f09372498.pdf](https://15a13b02-7dac-4315-baa5-b3ced1ea969d.filesusr.com/ugd/5518db_164bac27f4654b1f94d3472f09372498.pdf).

5. Stoiber M, Quick J, Egan R, Eun Lee J, Celniker S, Neely RK, et al. De novo Identification of DNA Modifications Enabled by Genome-Guided Nanopore Signal Processing. *bioRxiv*. 2017; Available from: <https://www.biorxiv.org/content/early/2017/04/10/094672>.
6. Tyson JR, James P, Stoddart D, Sparks N, Wickenhagen A, Hall G, et al. Improvements to the ARTIC multiplex PCR method for SARS-CoV-2 genome sequencing using nanopore. *bioRxiv*.
7. Zheng Z, Li S, Su J, Leung AWS, Lam TW, Luo R. Symphonizing pileup and full-alignment for deep learning-based long-read variant calling. *bioRxiv*. 2021; Available from: <https://www.biorxiv.org/content/early/2021/12/30/2021.12.29.474431>.
8. Shafin K, Pesout T, Chang PC, Nattestad M, Kolesnikov A, Goel S, et al. Haplotype-aware variant calling with PEPPER-Margin-DeepVariant enables high accuracy in nanopore long-reads. *Nature Methods*. 2021;18:1322–1332.
9. Luo R, Wong CL, Wong YS, Tang CI, Liu CM, Leung CM, et al. Exploring the limit of using a deep neural network on pileup data for germline variant calling. *Nature Machine Intelligence*. 2020;2(4):220–227.
10. Luo R, Sedlazeck FJ, Lam TW, Schatz MC. Clairvoyante: a multi-task convolutional deep neural network for variant calling in single molecule sequencing. *bioRxiv*. 2018;p. 310458.
11. Poplin R, Chang PC, Alexander D, Schwartz S, Colthurst T, Ku A, et al. A universal SNP and small-indel variant caller using deep neural networks. *Nature biotechnology*. 2018;36(10):983–987.
12. Robinson JT, Thorvaldsdóttir H, Winckler W, Guttman M, Lander ES, Getz G, et al. Integrative genomics viewer. *Nature biotechnology*. 2011;29(1):24–26.
13. Gotoh O. An improved algorithm for matching biological sequences. *Journal of Molecular Biology*. 1982;162(3):705–708. Available from: <https://www.sciencedirect.com/science/article/pii/0022283682903989>.
14. Shafin K. ONT R9.4.1 Guppy 5.0.7 sup HG003 whole genome performance evaluation against Clair3; 2021. Available from: [https://github.com/kishwarshafin/pepper/blob/r0.7/docs/performance\\_evaluation/Oxford\\_nanopore\\_r9\\_whole\\_genome.md](https://github.com/kishwarshafin/pepper/blob/r0.7/docs/performance_evaluation/Oxford_nanopore_r9_whole_genome.md).
15. Thompson JD. Introducing variable gap penalties to sequence alignment in linear space. *Bioinformatics*. 1995;11(2):181–186.
16. Smith RF, Smith TF. Pattern-induced multi-sequence alignment (PIMA) algorithm employing secondary structure-dependent gap penalties for use in comparative protein modelling. *Protein Engineering, Design and Selection*. 1992;5(1):35–41.
17. Shi J, Blundell TL, Mizuguchi K. FUGUE: sequence-structure homology recognition using environment-specific substitution tables and structure-dependent gap penalties. *Journal of molecular biology*. 2001;310(1):243–257.
18. Fischel-Ghodsian F, Mathiowitz G, Smith TF. Alignment of protein sequences using secondary structure: a modified dynamic programming method. *Protein Engineering, Design and Selection*. 1990;3(7):577–581.
19. Qiu J, Elber R. SSALN: An alignment algorithm using structure-dependent substitution matrices and gap penalties learned from structurally aligned protein pairs. *Proteins: Structure, Function, and Bioinformatics*. 2006;62(4):881–891.
20. Madhusudhan M, Marti-Renom MA, Sanchez R, Sali A. Variable gap penalty for protein sequence–structure alignment. *Protein Engineering Design and Selection*. 2006;19(3):129–133.
21. Goonesekere NC, Lee B. Frequency of gaps observed in a structurally aligned protein pair database suggests a simple gap penalty function. *Nucleic acids research*. 2004;32(9):2838–2843.
22. Sedlazeck FJ, Rescheneder P, Smolka M, Fang H, Nattestad M, Von Haeseler A, et al. Accurate detection of complex structural variations using single-molecule sequencing. *Nature methods*. 2018;15(6):461–468.
23. Highnam G, Franck C, Martin A, Stephens C, Puthige A, Mittelman D. Accurate human microsatellite genotypes from high-throughput resequencing data using informed error profiles. *Nucleic acids research*. 2013;41(1):e32–e32.
24. Cao MD, Tasker E, Willadsen K, Imelfort M, Vishwanathan S, Sureshkumar S, et al. Inferring short tandem repeat variation from paired-end short reads. *Nucleic acids research*. 2014;42(3):e16–e16.
25. Ummat A, Bashir A. Resolving complex tandem repeats with long reads. *Bioinformatics*. 2014;30(24):3491–3498.
26. Wright C. Medaka; 2020. Medaka - Medaka 1.2.0 documentation. Available from: <https://nanoporetech.github.io/medaka/>.
27. Institute B. Indel-based Realignment: Improving the original alignments of the reads based on multiple sequence (re-)alignment; 2016. GATK talks. Available from: <https://qcb.ucla.edu/wp-content/uploads/sites/14/2016/03/GATKwr12-3-IndelRealignment.pdf>.



28. Kojima K, Kawai Y, Misawa K, Mimori T, Nagasaki M. STR-realigner: a realignment method for short tandem repeat regions. *BMC genomics*. 2016;17(1):1–15.
29. Ryan CP. Tandem repeat disorders. *Evolution, Medicine, and Public Health*. 2019 01;2019(1):17–17. Available from: <https://doi.org/10.1093/emph/eoz005>.
30. Needleman SB, Wunsch CD. A general method applicable to the search for similarities in the amino acid sequence of two proteins. *Journal of molecular biology*. 1970;48(3):443–453.
31. Altschul SF, Erickson BW. Optimal sequence alignment using affine gap costs. *Bulletin of mathematical biology*. 1986;48(5-6):603–616.
32. Krusche P, Trigg L, Boutros PC, Mason CE, Francisco M, Moore BL, et al. Best practices for benchmarking germline small-variant calls in human genomes. *Nature biotechnology*. 2019;37(5):555–560.
33. Fan H, Chu JY. A brief review of short tandem repeat mutation. *Genomics, proteomics & bioinformatics*. 2007;5(1):7–14.
34. Technologies ON. *kmer\_models*. GitHub repository. 2017;.
35. Group TSFSW. Sequence Alignment/Map (SAM) Format Specification; 2021. Available from: <https://samtools.github.io/hts-specs/SAMv1.pdf>.
36. Suzuki H, Kasahara M. Acceleration of nucleotide semi-global alignment with adaptive banded dynamic programming. *BioRxiv*. 2017;p. 130633.
37. Technologies ON. Rebasecalling of SRE and ULK GM24385 Dataset; 2021. Available from: [https://labs.epi2me.io/gm24385\\_2021.05/](https://labs.epi2me.io/gm24385_2021.05/).
38. Li H. Minimap2: pairwise alignment for nucleotide sequences. *Bioinformatics*. 2018;34(18):3094–3100.
39. Martin M, Patterson M, Garg S, Fischer S, Pisanti N, Klau GW, et al. WhatsHap: fast and accurate read-based phasing. *BioRxiv*. 2016;p. 085050.